



Co-delivery of doxorubicin and paclitaxel by PEG-polypeptide nanovehicle for the treatment of non-small cell lung cancer



Shixian Lv^{a,e}, Zhaohui Tang^a, Mingqiang Li^{a,e}, Jian Lin^{a,e}, Wantong Song^a, Huaiyu Liu^c, Yubin Huang^d, Yuanyuan Zhang^{b,**}, Xuesi Chen^{a,*}

^aKey Laboratory of Polymer Ecomaterials, Changchun Institute of Applied Chemistry, Chinese Academy of Sciences, Changchun 130022, PR China

^bWake Forest Institute for Regenerative Medicine, Wake Forest School of Medicine, Medical Center Boulevard, Winston-Salem, NC 27157, USA

^cLaboratory Animal Center, Jilin University, Changchun 130012, PR China

^dState Key Laboratory of Polymer Physics and Chemistry, Changchun Institute of Applied Chemistry, Chinese Academy of Sciences, Changchun 130022, PR China

^eUniversity of Chinese Academy of Sciences, Beijing 100039, PR China

ARTICLE INFO

Article history:

Received 18 February 2014

Accepted 11 April 2014

Available online 1 May 2014

Keywords:

Chemotherapy
Drug co-delivery
Nanoparticle
Polypeptide
Controlled drug release

ABSTRACT

Despite progress, combination therapy of different functional drugs to increase the efficiency of anti-cancer treatment still remains challenges. An amphiphilic methoxy poly(ethylene glycol)-*b*-poly(L-glutamic acid)-*b*-poly(L-lysine) triblock copolymer decorated with deoxycholate (mPEEG-*b*-PLG-*b*-PLL/DOCA) was synthesized and developed as a nanovehicle for the co-delivery of anticancer drugs: doxorubicin (DOX) and paclitaxel (PTX). The amphiphilic copolymer spontaneously self-assembled into micellar-type nanoparticles in aqueous solutions and the blank nanoparticles possessed excellent stability. Three different domains of the copolymer performed distinct functions: PEG outer corona provided prolonged circulation, middle biodegradable and hydrophilic PLG shell was designed for DOX loading through electrostatic interactions, and hydrophobic deoxycholate modified PLL served as the container for PTX. *In vitro* cytotoxicity assays against A549 human lung adenocarcinoma cell line demonstrated that the DOX + PTX co-delivered nanoparticles (Co-NPs) exhibited synergistic effect in inducing cancer cell apoptosis. *Ex vivo* DOX fluorescence imaging revealed that Co-NPs had highly efficient targeting and accumulation at the implanted site of A549 xenograft tumor *in vivo*. Co-NPs exhibited significantly higher antitumor efficiency in reducing tumor size compared to free drug combination or single drug-loaded nanoparticles, while no obvious side effects were observed during the treatment, indicating this co-delivery system with different functional antitumor drugs provides the clinical potential in cancer therapy.

© 2014 Elsevier Ltd. All rights reserved.

1. Introduction

The combination therapy of multiple drugs with different action sites has been proved to be an effective strategy in clinical cancer treatments. This combination can not only delay the cancer adaptation process and related cancer cell mutations, but also reduce drug side effect by decreasing each of their doses and achieve synergistic therapeutic efficacy [1–5]. However, it is difficult to combine free drugs to obtain optimal anticancer effect due to their

different biochemical activities and pharmacokinetics among these drugs [6]. In addition, the combination of free drugs often brought more serious toxic side effects to human bodies, which has become a serious problem in clinical cancer treatments [7].

Over the past few decades, the nano-scaled drug carriers based on amphiphilic copolymers have been attracting great attention for the chemotherapeutic drug delivery in cancer treatment. With synthetic versatility and proper structure design, the polymeric nanomedicines generally have befitting size distribution, good biocompatibility, higher stability, controllable drug release profiles, altered pharmacokinetics and body biodistribution, which offer the great advantages over traditional therapeutic agents. Because these traditional anticancer drugs are limited in use due to fast degradation, undesirable drug uptake by normal organs and serious systemic toxicity [8,9]. In addition, the nano-scaled drug carriers

* Corresponding author. Tel./fax: +86 431 85262112.

** Corresponding author. Tel.: +1 336 713 1189; fax: +1 336 713 7290.

E-mail addresses: yzhang@wakehealth.edu (Y. Zhang), xschen@ciac.ac.cn (X. Chen).

also achieve better accumulation in solid tumors through the enhanced permeability and retention (EPR) effect as compared with free drugs [10]. Accordingly, several promising nanomedicines have been adopted in clinical trials, e.g., Doxil® (liposomal DOX), Abraxane (protein-bound paclitaxel), Genexol-PM (paclitaxel-encapsulated polymeric micelles) [11–13]. However, most of the current nanomedicines only load a single drug, which rapidly develop drug resistance in tumor cells [14].

Nanocarriers provide the possibility to simultaneously deliver multiple therapeutic agents. Compared to the combination of free drugs, the combination of two or more drugs within a single nanocarrier can overcome toxicity and other side effects. Furthermore, such multiagent systems guarantee the simultaneous delivery of sufficient amount of drugs to tumor site, ensure the synergistic effect and the improved antitumor efficacy [7,15]. However, the distinct water solubility and the diverse electric properties of chemotherapeutic drugs make it difficult to co-deliver multi-drugs. For instance, doxorubicin (DOX) and paclitaxel (PTX), which are among the most common used chemotherapeutic drugs in clinic against various solid tumors, have remarkably large differences in their water solubility properties and anticancer mechanisms. Doxorubicin (DOX) is one of the most effective anthracycline antitumor drugs which can interfere with DNA through insertion and then induce cancer cell apoptosis. Clinical commonly used DOX is hydrophilic in the form of protonated doxorubicin hydrochloride (DOX·HCl). PTX, a representative antimicrotubule agent, is highly hydrophobic with extremely poor water solubility [16]. Even the combination of DOX and PTX has been used as the first-line treatment for metastatic breast cancer with increased tumor regression rates compared the individual drugs, but the co-delivery of DOX and PTX was rarely investigated [17–19]. Wang et al. employed amphiphilic methoxy PEG-PLGA copolymer nanoparticles as carriers to co-deliver DOX and PTX through a double emulsion method and received a synergistic

antitumor effect *in vitro*. However, the stability of such polymer/drug interactions between cationic DOX molecules and uncharged PEG-PLGA copolymers is highly desired [2]. The system above was still devoid of data to prove the *in vivo* feasibility of their co-delivery systems.

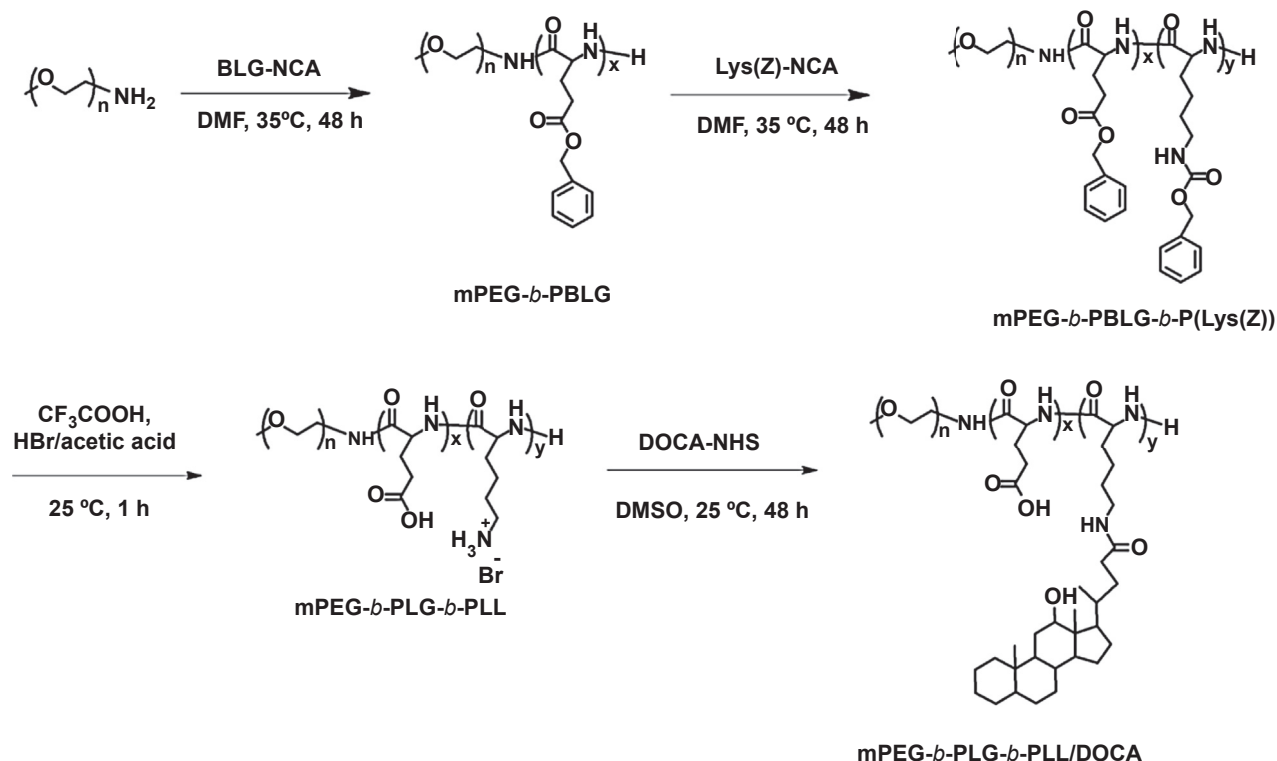
In order to co-deliver multiple antitumor drugs with strong polymer/drug interactions and robust construct stability, an amphiphilic triblock copolymer, methoxy poly(ethylene glycol)-*b*-poly(L-glutamic acid)-*b*-poly(L-lysine) decorated with deoxycholate (mPEG-*b*-PLG-*b*-PLL/DOCA) was designed and utilized as a favorable carrier for the co-delivery of DOX and PTX in this study. The mPEG-*b*-PLG-*b*-PLL/DOCA copolymers are expected to undergo spontaneous self-assembling to nanomicelles in the aqueous solutions resulting in the PEG outer corona, PLG middle shell and hydrophobic PLL/DOCA inner core. The PEG block provides the prolonged blood circulation of the nanoparticles by reducing non-specific interactions with blood components. The anionic poly (glutamic acid) provides the strong electrostatic interaction with cationic DOX·HCl. Such polymer/drug complexes through electrostatic interactions have been proved to be very effective in our previous studies [20–22]. The hydrophobic modified PLL component serves as a reservoir for lipophilic drug.

The physiochemical properties, stability, self-assembly, *in vitro* drug release behavior were investigated. The synergistic antitumor effect of the DOX and PTX co-delivered mPEG-*b*-PLG-*b*-PLL/DOCA nanoparticles (Co-NPs) was evaluated both *in vitro* and *in vivo*.

2. Materials and methods

2.1. Materials

Poly(ethylene glycol) monomethyl ether (mPEG, $M_n = 5000$, Aldrich), doxorubicin hydrochloride and paclitaxel (DOX·HCl and PTX, Beijing Huafeng United Technology Corporation), 3-(4,5-dimethyl-thiazol-2-yl)-2,5-diphenyl tetrazolium bromide (MTT, Sigma), 4',6-diamidino-2-phenylindole dihydrochloride (DAPI, Sigma), fluorescein isothiocyanate (FITC, Aladdin), Cy5.5-NHS ester (Lumiprobe) and



Scheme 1. Synthesis pathway of mPEG-*b*-PLG-*b*-PLL/DOCA.

N^ε-benzyloxycarbonyl-L-lysine (H-Lys(Z)-OH, GL Biochem Co. Ltd.) were used as received. *N,N*-dimethylformamide (DMF) and dimethylsulfoxide (DMSO) were stored over calcium hydride (CaH₂) and purified by vacuum distillation with CaH₂. Amino-terminated poly(ethylene glycol) methyl ether (mPEG-NH₂) and γ -Benzyl-L-glutamate-*N*-carboxyanhydride (BLG-NCA) were prepared according to our previous work [23]. *N*^ε-benzyloxycarbonyl-L-lysine-*N*-carboxyanhydride (Lys(Z)-NCA) was synthesized as the literature report [24]. Succinimido deoxycholate (DOCA-NHS) was synthesized according to the literature [25].

2.2. Synthesis of mPEG-*b*-PLG-*b*-PLL triblock copolymer

Methoxy poly(ethylene glycol)-*b*-poly(L-glutamic acid)-*b*-poly(L-lysine) (mPEG-*b*-PLG-*b*-PLL) triblock copolymer was synthesized via the one-pot two-step ring-opening polymerization (ROP) of BLG-NCA and Lys(Z)-NCA monomers with mPEG-NH₂ as the macroinitiator and a subsequent deprotection of benzyl groups. In brief, mPEG-NH₂ (4.00 g, 0.8 mmol) was dissolved in dry DMF (40 mL) after azeotropic dehydration process with toluene, then BLG-NCA (2.31 g, 8.8 mmol) dissolved in dry DMF (23 mL) was added via a syringe under argon. The reaction was maintained at 35 °C under argon. After 2 days, a trace of solution was removed from the system and precipitated into ice diethyl ether for ¹H NMR and GPC measurements of methoxy poly(ethylene glycol)-*b*-poly(γ -benzyl-L-glutamate) (mPEG-*b*-PBLG). Then, Lys(Z)-NCA (2.45 g, 8.0 mmol) was added, and the reaction was maintained for another 2 days. The methoxy poly(ethylene glycol)-*b*-poly(γ -benzyl-L-glutamate)-*b*-poly(*N*^ε-benzyloxycarbonyl-L-lysine) (mPEG-*b*-PBLG-*b*-P(Lys(Z))) triblock copolymer was obtained by the repeated precipitation from DMF into excess amount of ice diethyl ether. Yield: 86%.

Subsequently, mPEG-*b*-PBLG-*b*-P(Lys(Z)) (4.0 g) was dissolved in trifluoroacetic acid (TFA, 40 mL) at 0 °C in a flask. And then 12 mL HBr/acetic acid (33 wt%) was added slowly and the solution was stirred at 25 °C to remove the protecting groups. The mPEG-*b*-PLG-*b*-PLL copolymer was isolated by precipitation into excess amount of ice diethyl ether. After dried under vacuum, the crude product was purified by dialysis against distilled water (MWCO = 3500 Da) and freeze-dried to give the pure mPEG-*b*-PLG-*b*-PLL product, yielding a white solid. Yield: 90.0%.

2.3. Synthesis of mPEG-*b*-PLG-*b*-PLL/DOCA

Deoxycholate decorated methoxy poly(ethylene glycol)-*b*-poly(L-glutamic acid)-*b*-poly(L-lysine) (mPEG-*b*-PLG-*b*-PLL/DOCA) was synthesized by chemical coupling of mPEG-*b*-PLG-*b*-PLL with DOCA-NHS. In brief, mPEG-*b*-PLG-*b*-PLL (0.82 g, 0.1 mmol) and DOCA-NHS (0.44 g, 0.9 mmol) were dissolved in dry DMSO (15 mL), then triethylamine (TEA) (0.275 mL, 1.9 mmol) was added into the solution. The reaction mixture was maintained for 48 h at room temperature under a dry argon atmosphere. The mixture then was dialyzed (MWCO 3500 Da) against DMSO to remove unreacted small molecules and further dialyzed against distilled water to remove DMSO. The mPEG-*b*-PLG-*b*-PLL/DOCA white powder was obtained after lyophilization.

Table 1
Characterization of the copolymers.

Copolymer	Feed ratio	Composition ratio ^a	<i>M_n</i> ^a /10 ³ (g mol ⁻¹)	PDI ^b
mPEG- <i>b</i> -PBLG	113:11	113:11	7.2	1.08
mPEG- <i>b</i> -PBLG- <i>b</i> -P(Lys(Z))	113:11:10	113:10:9	9.6	1.10
mPEG- <i>b</i> -PLG- <i>b</i> -PLL	—	113:10:9	8.2	—

^a Estimated by ¹H NMR.

^b Measured by GPC.

To label mPEG-*b*-PLG-*b*-PLL/DOCA with FITC, mPEG-*b*-PLG-*b*-PLL/DOCA (50 mg) and FITC (5 mg) were dissolved in dry DMF and the solution was stirred for 24 h at room temperature in dark. Then the mixture was dialyzed against distilled water and freeze-dried. The FITC-labeled mPEG-*b*-PLG-*b*-PLL/DOCA was obtained as a yellow powder.

2.4. Preparation of drug-loaded nanoparticles

The DOX-loaded mPEG-*b*-PLG-*b*-PLL/DOCA nanoparticles (DOX-NPs) were prepared according to our previous report [21]. Briefly, mPEG-*b*-PLG-*b*-PLL/DOCA (90 mg) was dissolved in distilled water and adjusted to pH 7.0–7.5, then DOX-HCl (10 mg) dissolved in distilled water was added dropwise. After stirring overnight in the dark, the free DOX was removed by dialysis using a dialysis bag (MWCO 3500 Da) against deionized water for 24 h, and then freeze-dried to obtain the DOX-NPs powders.

The PTX-loaded mPEG-*b*-PLG-*b*-PLL/DOCA nanoparticles (PTX-NPs) were prepared by a dialysis method. Briefly, 95 mg of mPEG-*b*-PLG-*b*-PLL/DOCA and 5 mg of PTX were dissolved in 4.0 mL of DMSO, and the solution was allowed to stir at 25 °C for 4 h. Then, the solution was added to 16.0 mL of deionized water dropwise under gentle stirring. After stirring for 12 h at 25 °C, the solution was dialyzed against excess deionized water with a dialysis bag (MWCO 3500) overnight, and then filtered through a 0.45 mm pore-sized microporous membrane. The PTX-NPs powders were obtained after lyophilization.

To prepare the DOX and PTX co-delivered mPEG-*b*-PLG-*b*-PLL/DOCA nanoparticles (Co-NPs), mPEG-*b*-PLG-*b*-PLL/DOCA (85 mg), DOX (10 mg) and PTX (5 mg) were dissolved in 4.0 mL of DMSO. Then, the solution was added to phosphate buffered saline (PBS) solution (pH = 7.0, 16.0 mL) under gentle stirring. The subsequent steps were identical with the preparation of PTX-NPs. FITC-labeled Co-NPs were prepared by the same procedure used to Co-NPs.

DOX inside the nanoparticles was determined by UV absorption at 480 nm. PTX loaded in the nanoparticles was determined by high-performance liquid chromatography (HPLC). The mobile phase consisted of a mixture of acetonitrile and water (4:1, v/v) using a Waters 1525 Binary HPLC pump, and the flow rate was 1.0 mL

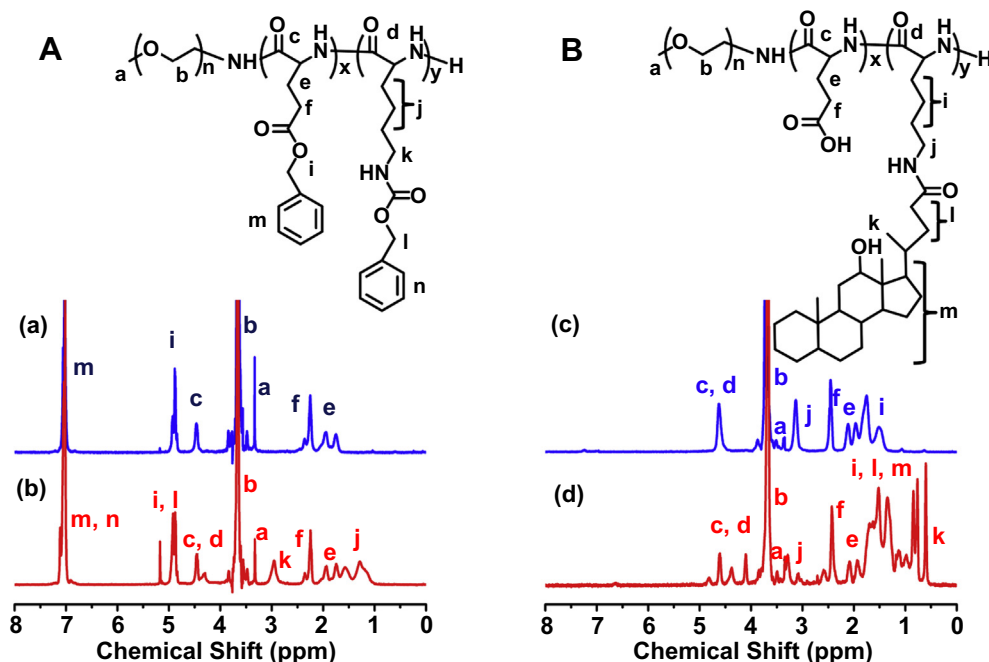


Fig. 1. Characterization of the copolymers. ¹H NMR spectra of mPEG-*b*-PBLG (a), mPEG-*b*-PBLG-*b*-P(Lys(Z)) (b), mPEG-*b*-PLG-*b*-PLL (c) and mPEG-*b*-PLG-*b*-PLL/DOCA (d) in CD₃COOD.

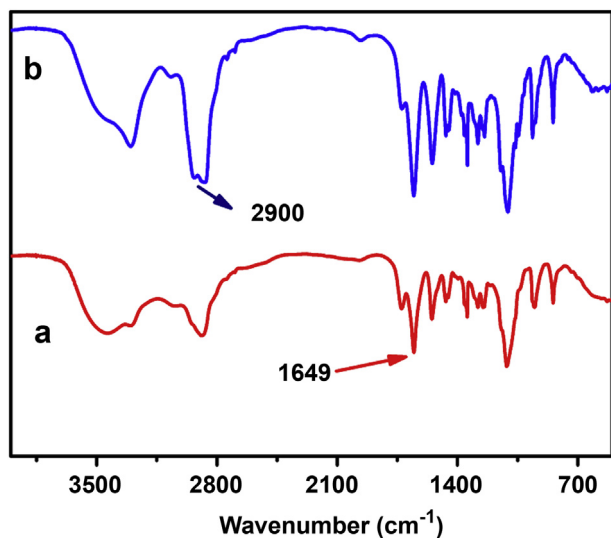


Fig. 2. Characterization of the copolymers. FT-IR spectra of mPEG-*b*-PLG-*b*-PLL (a) and mPEG-*b*-PLG-*b*-PLL/DOCA (b).

min^{-1} . 20 μL of sample was injected. The column effluent was detected at 227 nm with a Waters 2489 UV/Visible detector. The column type was Waters Symmetry[®] C18 (5 μm , 4.6 mm \times 250 mm). Drug loading content (DLC, wt%) and drug loading efficiency (DLE, wt%) were calculated according to the following formulas:

$$\text{DLC} = (\text{amount of loaded drug} / \text{amount of drug-loaded nanoparticles}) \times 100\%$$

$$\text{DLE} = (\text{amount of loaded drug} / \text{amount of feeding drug}) \times 100\%$$

2.5. Characterizations

The ¹H NMR, critical micelle concentration (CMC), zeta potential, dynamic laser scattering (DLS), transmission electron microscopy (TEM) measurements were performed as our previous reported [20,21]. FT-IR spectra were recorded

on a Bio-Rad Win-IR instrument using the potassium bromide method. Molecular weight distributions (polydispersity index, $\text{PDI} = M_w/M_n$) of the mPEG-*b*-PBLG and mPEG-*b*-PBLG-*b*-P(Lys(Z)) copolymers were determined by gel permeation chromatography (GPC) under the same test condition as our previous work [21].

2.6. In vitro drug release assay

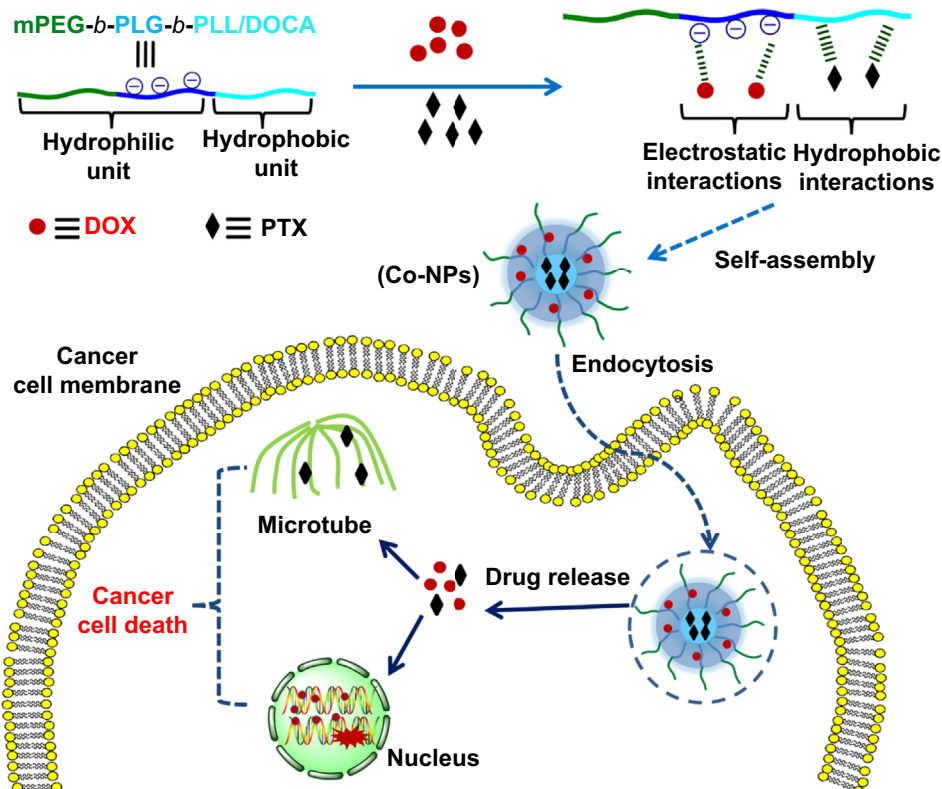
The release profiles of DOX and PTX from Co-NPs were assessed in PBS containing 0.1% (w/v) Tween 80 at different pH values (7.4 and 5.5) by the dialysis method. Briefly, the weighed Co-NPs were suspended in 5.0 mL of the PBS release medium and transferred into a dialysis bag (MWCO 3500 Da). The release experiment was started by placing the dialysis bag into 45.0 mL of release medium at 37 °C with continuous shaking at 110 rpm. At predetermined time, 4 mL of the incubated solution was withdrawn and replaced with equal volume of fresh PBS. The amount of DOX released was determined using UV-Vis spectrometer at 480 nm. PTX contents in the samples were measured by HPLC. The release experiments were conducted in triplicate.

2.7. Cell cultures

Three types of human cancer lines, including lung carcinoma (A549), cervical carcinoma (HeLa) and breast carcinoma (MCF-7) were cultured in Dulbecco's modified Eagle's medium (DMEM) with high glucose containing 10% fetal bovine serum (FBS), supplemented with 50 U mL^{-1} penicillin and 50 U mL^{-1} streptomycin, and incubated at 37 °C in 5% CO_2 atmosphere.

2.8. Confocal laser scanning microscopy (CLSM) observation

The cellular uptake behavior of FITC-labeled Co-NPs was determined by CLSM toward A549 cells. The cells were seeded on the coverslips in 6-well plates with a density of 1×10^5 cells per well in 2 mL of DMEM and cultured for 24 h, and then the original medium was replaced with free DOX and FITC-labeled Co-NPs (at a DOX concentration of 5 $\mu\text{g mL}^{-1}$ in 2 mL of DMEM). After 1 or 3 h incubation, the cells were washed and fixed with 4% formaldehyde for 20 min at room temperature. The cell nuclei were stained by DAPI according to the standard protocol provided by the supplier. The coverslips were placed onto the glass microscope slides. The subcellular localization and intracellular DOX release of Co-NPs were visualized under a laser scanning confocal microscope (Carl Zeiss LSM 700).



Scheme 2. Schematic illustrations of antitumor drug loading and intracellular performance of Co-NPs.

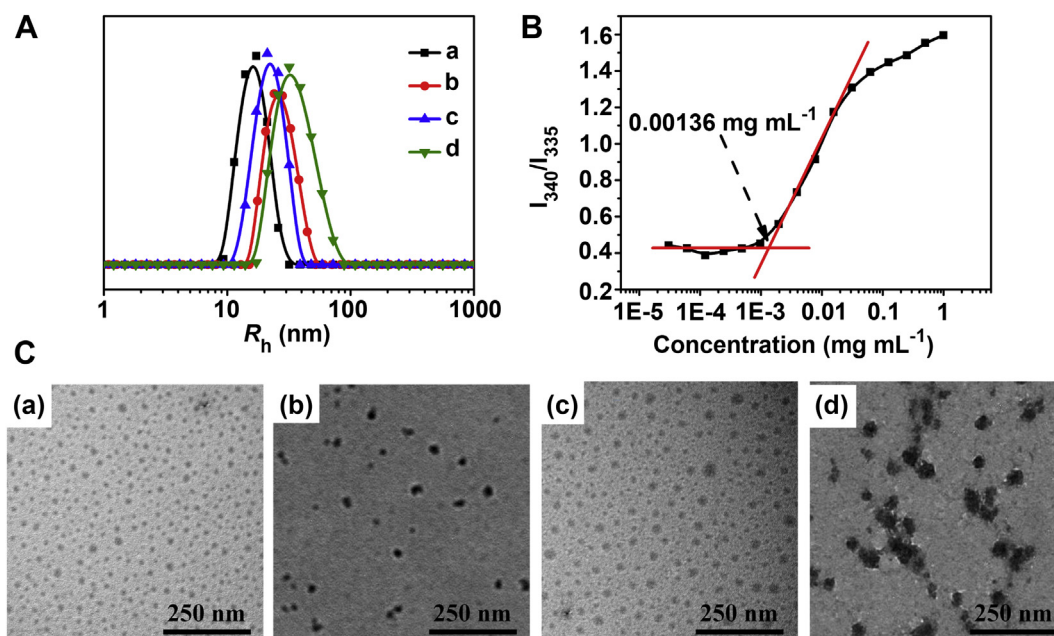


Fig. 3. Solution behaviors of the nanoparticles. (A) Hydrodynamic radii (R_h) of blank mPEG-*b*-PLG-*b*-PLL/DOCA nanoparticles (a), DOX-NPs (b), PTX-NPs (c) and Co-NPs (d) in PBS estimated by and DLS. (B) Critical micelle concentration (CMC) of mPEG-*b*-PLG-*b*-PLL/DOCA nanoparticles using pyrene as a fluorescence probe. (C) Typical TEM images of blank mPEG-*b*-PLG-*b*-PLL/DOCA nanoparticles (a), DOX-NPs (b), PTX-NPs (c) and Co-NPs (d).

2.9. *In vitro* cytotoxicity assays

The *in vitro* cytotoxicities of mPEG-*b*-PLG-*b*-PLL/DOCA, free drugs, and drug-loaded nanoparticles on three types of cancer cell lines were assessed by MTT assay.

A549, HeLa or MCF-7 cells were seeded in 96-well plates at 7000 cells per well in 100 μ L of DMEM medium and incubated at 37 $^{\circ}$ C in a 5% CO_2 atmosphere for 24 h, followed by removing culture medium and then adding mPEG-*b*-PLG-*b*-PLL/DOCA blank nanoparticles (200 μ L in DMEM medium) at the different concentrations. The cells were subjected to MTT assay after being incubated for another 48 h. The absorbency of the solution was measured on a Bio-Rad 680 microplate reader at 492 nm. The relative cell viability was calculated by $(A_{\text{sample}}/A_{\text{control}}) \times 100$, where A_{sample} and A_{control} denoted as the absorbances of the sample well and control well, respectively. Data are presented as average \pm SD ($n = 3$).

Tumor cell proliferation inhibition behaviors of free drugs and drug-loaded micelles were evaluated against human lung adenocarcinoma A549 cells following the similar procedure, and 48 h incubation time was applied. The inhibitory concentration (IC_x) values were determined using Origin 8.0 (OriginLab, Northampton, MA) according to the fitted data. The Combination Index (CI) was measured according to the Chou and Talalay's method [26]. To distinguish synergistic, additive, or antagonistic cytotoxic effects, the following equation was used:

$$\text{CI}_x = \frac{(D)_1}{(D_x)_1} + \frac{(D)_2}{(D_x)_2}$$

$(D_x)_1$ and $(D_x)_2$ represent the IC_x value of drug 1 alone and drug 2 alone, respectively. $(D)_1$ and $(D)_2$ represent the concentration of drug 1 and drug 2 in the combination system at the IC_x value. $\text{CI} > 1$ represents antagonism, $\text{CI} = 1$ represents additive and $\text{CI} < 1$ represents synergism. In this work, IC_{50} (inhibitory concentration to produce 50% cell death) was applied.

Table 2
Characterization of the nanoparticles.

Entry	R_h (nm) ^a at 25 $^{\circ}$ C	Zeta potential ^b (mV)	DLC of PTX ^c (wt%)	DLE of PTX (%)	DLC of DOX ^d (wt%)	DLE of DOX (%)
Blank nanoparticles	16.7 \pm 4.0	-23.4 \pm 3.4	—	—	—	—
DOX-NPs	27.6 \pm 7.0	-18.3 \pm 1.3	—	—	9.58	95.8
PTX-NPs	22.5 \pm 5.4	-22.7 \pm 2.2	2.12	42.4	—	—
Co-NPs	36.7 \pm 12.5	-18.20 \pm 1.99	2.24	44.8	8.49	84.9

^a Measured by DLS.

^b Estimated at pH 7.4 at 25 $^{\circ}$ C, a mean \pm STD of 6 measurements.

^c Determined by HPLC.

^d Determined by UV absorption at 480 nm.

2.10. Animals

Male Balb/C nude mice (6–8 weeks old) were purchased from the Experimental Animal Center, Chinese Academy of Sciences (Shanghai, China). The animals were maintained in specific pathogen free (SPF) animal lab. Animal Care and Use Committee of Jilin University approved to use the animals in this study.

2.11. Excised imaging

The mice bearing A549 tumor were injected with free DOX and Co-NPs *via* tail vein (5 mg DOX/kg). After the injection, mice were sacrificed at 3, 10 and 24 h, the tumor and major organs (heart, kidney, liver, lung and spleen) were collected and washed with PBS. At each time point, three mice were used. The excised organs were visualized using a Maestro *in vivo* Imaging System (Cambridge Research & Instrumentation, Inc., Woburn, MA, USA) at excitation and emission wavelengths of 523 and 560 nm, respectively.

2.12. *In vivo* antitumor efficiency

A human non-small cell lung cancer xenograft tumor model was generated by the subcutaneous injection of A549 cells (1.5×10^6 , 100 μ L in PBS) in the right flank of each mouse. When the tumor volume reached approximately 20–50 mm^3 , mice were randomly divided into 7 groups (G) ($n = 6$), the treatment was started and this day was designated as day 0. Mice were treated with PBS (G1), free DOX-HCl (4 mg kg^{-1} , G2), DOX-NPs (4 mg DOX kg^{-1} , G3), free PTX (1 mg kg^{-1} , G4), PTX-NPs (1 mg PTX kg^{-1} , G5), free DOX + PTX (4 mg DOX kg^{-1} and 1 mg PTX kg^{-1} , G6) and Co-NPs (4 mg DOX kg^{-1} and 1 mg PTX kg^{-1} , G7) intravenously *via* tail vein on days 0, 4, 8, and 12. Tumor volume and body weight were measured every other day to evaluate the antitumor activities and systematic toxicities of various formulations. The estimated tumor volume (mm^3) was calculated based on the following equation: $V = a \cdot b^2/2$, where a and b represented the longest and shortest diameter of the

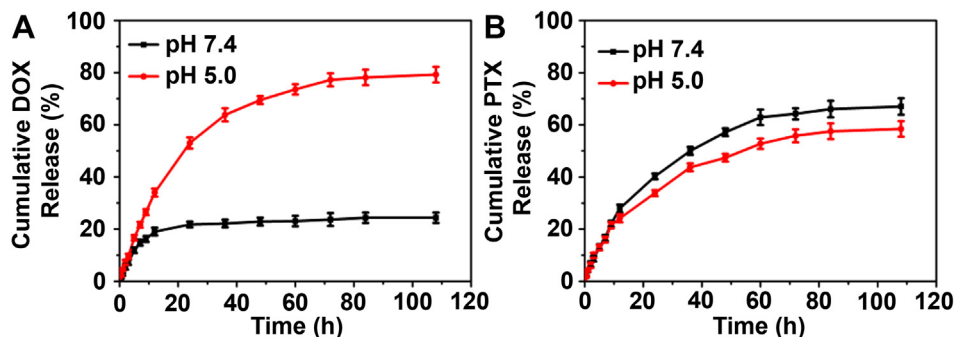


Fig. 4. Drug release curves of anticancer drugs *in vitro* over time. Levels of DOX (A) and PTX (B) from Co-NPs in PBS containing 0.1% (w/v) Tween 80 were released at various pH values (7.4 and 5.0) at 37 °C. Each point was an average of three measurements.

tumors. At day 18, mice were sacrificed. The tumors and major organs, including heart, liver, spleen, lung and kidney were excised for histopathology analyses.

2.13. Histopathology and immunohistochemical analysis

At day 18, mice were anesthetized and the chests were excised open, PBS and paraformaldehyde solution (4% in PBS) were perfused from the left atrium. Tumors were removed and fixed in 4% buffered paraformaldehyde overnight, and then embedded in paraffin. The paraffin-embedded tissue samples of the implanted tumor were sliced at 5 μ m thickness, and stained with hematoxylin and eosin (H&E) for histopathological changes evaluated by microscope (Nikon TE2000U).

The immunohistochemical evaluation was performed with rabbit monoclonal primary antibody for cleaved PARP (Abcam, Cambridge, MA, USA) and PV-6000 two-step immunohistochemistry kit (polymer detection system for immuno-histological staining; Zhongshan Goldbridge Biotechnology, Beijing, China).

In situ terminal deoxynucleotidyl transferase-mediated UTP end labeling (TUNEL) assay was performed using a FragEL™ DNA fragment detection kit

(colorimetric-TdT Enzyme method) according to the manufacturer's protocol (EMD chemicals Inc, Darmstadt, Germany).

2.14. Statistical analysis

All experiments were performed at least three times and expressed as means \pm SD. Statistical significances were analyzed using the Student's *t*-test. $P < 0.05$ was considered statistically significant, and $P < 0.01$ was considered highly significant.

3. Results and discussion

3.1. Synthesis of copolymers

For co-delivery of DOX and PTX, mPEG-*b*-PLG-*b*-PLL/DOCA amphiphilic copolymer was synthesized (Scheme 1). The poly

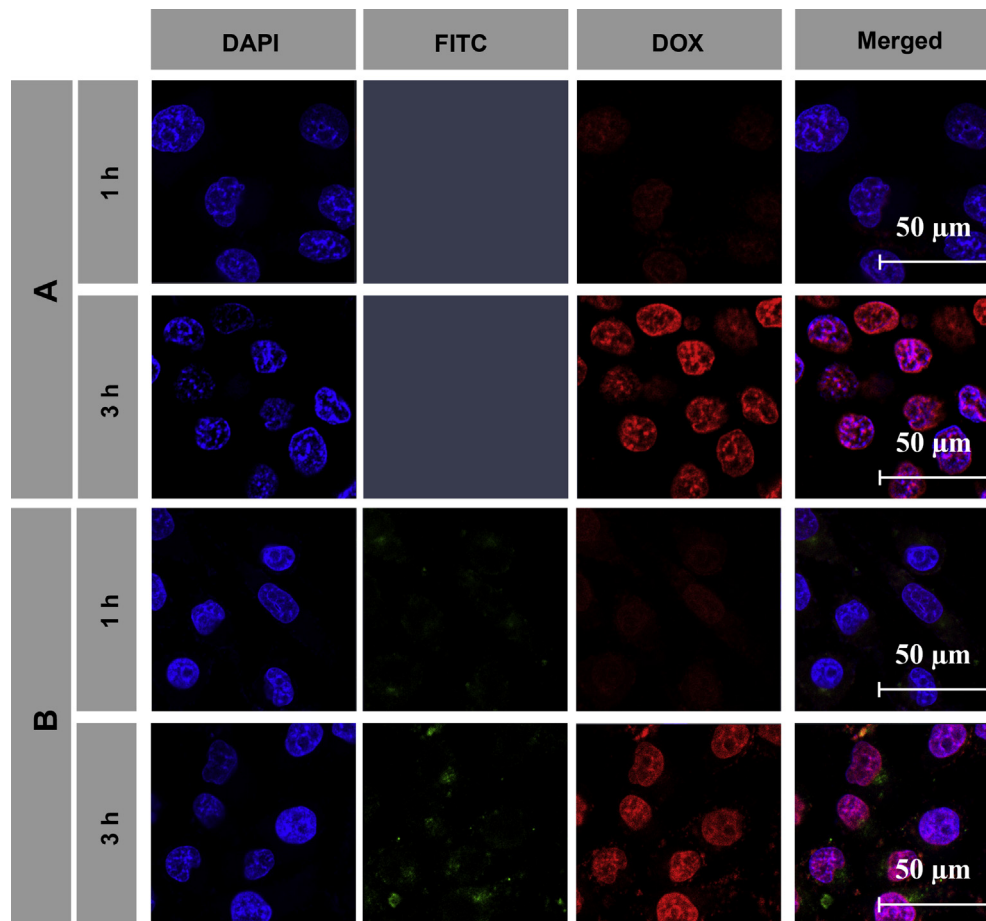


Fig. 5. Confocal laser scanning microscopy images of A549 cells after incubation with free DOX (A) and FITC-labeled Co-NPs (B) for 1 h and 3 h.

(glutamic acid) block provides the strong electrostatic interaction to load cationic DOX·HCl. The hydrophobic modified PLL domain serves as a reservoir for PTX through hydrophobic interaction. The mPEG-*b*-PLG-*b*-PLL triblock copolymers were first synthesized via the one-pot two-step ring-opening copolymerization of BLG-NCA and Lys(Z)-NCA using mPEG-NH₂ as the macroinitiator, followed by deprotecting the protection groups in HBr/acetic acid. The ¹H NMR spectra in trifluoroacetic acid-d (TFA-d) verified the successful synthesis of the resulting copolymers. All peaks of the copolymers were well assigned (Fig. 1). The degree of polymerization (DP) of BLG units in mPEG-*b*-PBLG-*b*-P(Lys(Z)) triblock copolymer was calculated to be 10 by comparing the integration of the methylene peak of the glutamate (–COCH₂–) with that of the methylene peak of poly(ethylene glycol) (–CH₂–CH₂–), which was nearly identical with the designed DP, indicating the high conversion efficiency of BLG-NCA monomer. The DPs of BLG and Lys(Z) units in mPEG-*b*-PBLG-*b*-P(Lys(Z)) triblock copolymer were determined to be 10 and 9, respectively, by comparing the integration of the methylene peak of the glutamate (–COCH₂–) and lysine (–CH₂–CH₂–CH₂–CH₂–NH) units with that of the methylene peak of poly(ethylene glycol) (–CH₂–CH₂–), demonstrating the successful synthesis of the triblock copolymer. After deprotection, the resonances at δ 4.87–4.92 ppm disappeared in the mPEG-*b*-PLG-*b*-PLL (Fig. 1c), revealing the complete deprotection of the γ-benzyl groups (C₆H₅CH₂–O–). The composition ratio of the monomeric repeating units in the copolymers did not change after deprotection of γ-benzyl (Table 1), suggesting that the deprotection reaction did not lead to the scission of poly(amino acids) backbones. GPC analyses revealed that both mPEG-*b*-PBLG and mPEG-*b*-PBLG-*b*-P(Lys(Z)) had a narrow molecular weight distribution (PDI = 1.10 and 1.08, respectively), which might be attributed to the living feature of the ROP of the NCA monomer.

mPEG-*b*-PLG-*b*-PLL/DOCA was further synthesized by the chemical coupling of mPEG-*b*-PLG-*b*-PLL with DOCA-NHS. The structure of mPEG-*b*-PLG-*b*-PLL/DOCA was characterized by ¹H NMR and FT-IR. As shown in Fig. 1c and d, the typical resonances of alkyl group in DOCA (δ 0.60, 0.76, 0.97 and 1.14 ppm) appeared in the ¹H NMR spectrum of mPEG-*b*-PLG-*b*-PLL/DOCA. By comparing the integration of the methyl peak of the DOCA at δ 0.60 with that of the methylene peak of poly(ethylene glycol) chain at δ 3.68, the DOCA groups decorated on each copolymer were calculated to be 8.33, which meant approximately 93% of the amino groups of the mPEG-*b*-PLG-*b*-PLL/DOCA copolymer had

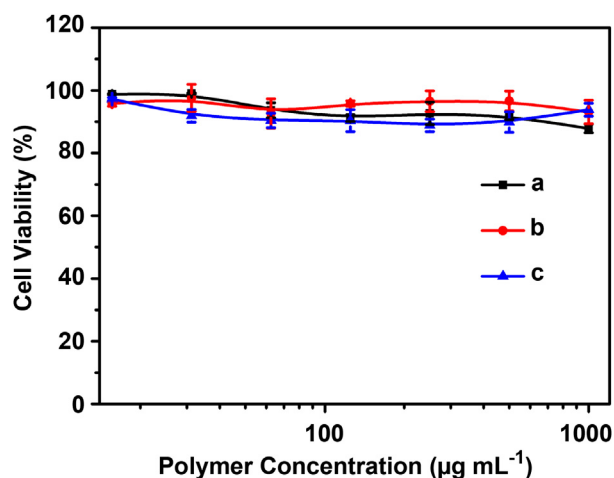


Fig. 6. Cell viabilities of different cell types after treated empty nanoparticles *in vitro*. A549 (a), HeLa (b) and MCF-7 (c) cells were incubated with blank mPEG-*b*-PLG-*b*-PLL/DOCA nanoparticles for 48 h before MTT assay ($n = 3$, mean \pm SD).

been converted into DOCA groups. And deoxycholate (DOCA) decoration was further confirmed by FT-IR, the FT-IR spectra of mPEG-*b*-PLG-*b*-PLL and mPEG-*b*-PLG-*b*-PLL/DOCA were listed on Fig. 2. The absorption at 1649 cm⁻¹ was attributed to the typical amide of poly(amino acid) chain on the copolymer (Fig. 2a), and the increased absorption of typical C–H stretching vibration at about 2900 cm⁻¹ induced by DOCA groups was observed from the FT-IR spectroscopy (Fig. 2b), indicating the successful synthesis of mPEG-*b*-PLG-*b*-PLL/DOCA.

3.2. Fabrication of the nanoparticles

Amphiphilic copolymers with hydrophilic and hydrophobic segments can self-assemble into various types of nanoparticles in aqueous solution, such as micelles and vesicles. In the study, the mPEG-*b*-PLG-*b*-PLL/DOCA triblock copolymers could self-assemble into micelles in the aqueous phase for loading DOX and PTX (Scheme 2). The DOX-NPs were prepared by simply mixing DOX and mPEG-*b*-PLG-*b*-PLL/DOCA in distilled water. The PTX-NPs and Co-NPs were prepared by a nanoprecipitation technique which was

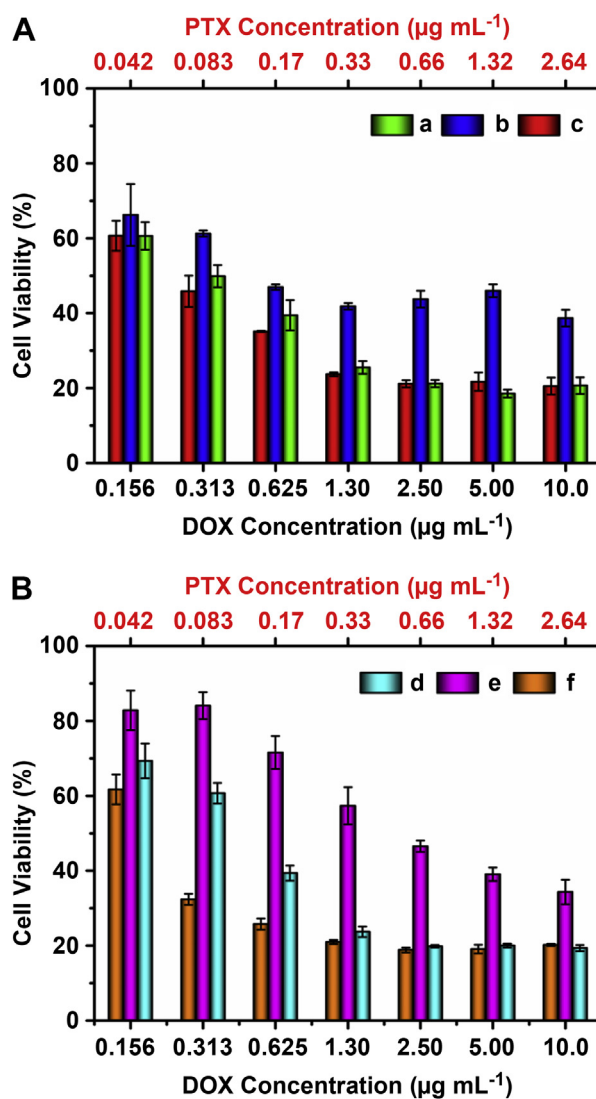


Fig. 7. Cell viabilities of lung cancer cells after treatment with different anticancer strategies *in vitro*. The A549 cancer cells were incubated with free DOX (a), free PTX (b), free DOX&PTX (c), DOX-NPs (d), PTX-NPs (e) and Co-NPs (f) for 48 h. Data were presented as the mean \pm standard deviation ($n = 3$).

Table 3

In vitro cytotoxicities and combination index (CI) of drug formulations against A549 cells for 48 h incubation time.

Entry	IC ₅₀ DOX/($\mu\text{g mL}^{-1}$)	IC ₅₀ PTX/($\mu\text{g mL}^{-1}$)	CI ₅₀
Free DOX	0.312	–	–
Free PTX	–	0.151	–
DOX + PTX	0.260	0.068	1.28
DOX-NPs	0.438	–	–
PTX-NPs	–	0.541	–
Co-NPs	0.206	0.054	0.571

similar to the literature [27,28]. The DLC and DLE for the drug-loaded nanoparticles were listed in Table 1. The Co-NPs had a DOX loading content of 8.49 wt.% and a PTX loading content of 2.24%, indicating that DOX and PTX were successfully co-loaded into the mPEG-*b*-PLG-*b*-PLL/DOCA nanoparticles. The size distributions of the nanoparticles were determined by DLS measurements. As shown in Fig. 3A, the blank mPEG-*b*-PLG-*b*-PLL/DOCA nanoparticles had a narrow distribution with a hydrodynamic radius (R_h) of 16.7 ± 4.0 nm, and the sizes of the drug-loaded nanoparticles were listed in Table 2. All the drug-loaded nanoparticles had hydrodynamic radii of 20–40 nm. Loading of drug

led to increase of the particle size, while maintained a narrow distribution (Fig. 3A). The morphologies of the nanoparticles were measured by TEM measurement. TEM images revealed that all nanoparticles possessed uniformly spherical morphologies (Fig. 3C). The sizes from TEM observations were slightly smaller than that from DLS measurements, which might be attributed to the dehydration of nanoparticles during the TEM sample preparation and shrinkage of the mPEG shell.

CMC is a key factor to determine the stability of nanoparticles in the medium. In this study, CMC is measured by fluorescence spectroscopy using pyrene as a probe, which exhibits a peak shift in its excitation spectrum when it is captured into a hydrophobic inner core. The CMC value was calculated from the inflection point of fluorescence intensity ratio of I_{340}/I_{335} (Fig. 3B) as a function of the logarithm concentration of the nanoparticles according to the literature [29]. The blank mPEG-*b*-PLG-*b*-PLL/DOCA nanoparticles had an extremely low CMC of $0.00136 \text{ mg mL}^{-1}$, indicating the mPEG-*b*-PLG-*b*-PLL/DOCA nanoparticles exhibited great stability against dilution. Such low CMC value could guarantee the nanoparticles to retain their construct during the *in vivo* diluted conditions (e.g. blood stream), which is great benefit for the effective delivery to tumors. The surface zeta potentials of the blank and drug-loaded nanoparticles were measured on a Zeta Potential/BI-

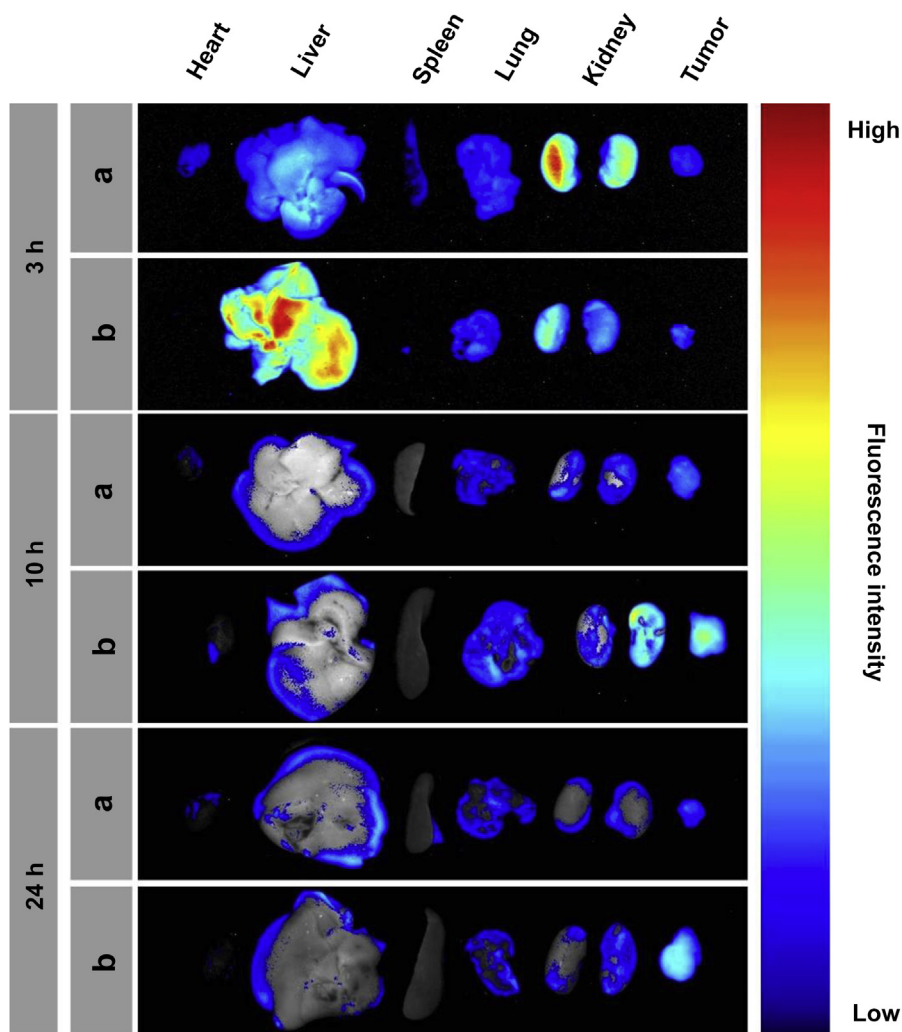


Fig. 8. Anticancer drugs distributed in solid organs and targeted at the implanted A549 lung cancer tumor *in vivo* at different time points. *Ex vivo* DOX fluorescence imaging of A549 tumor-bearing nude mice was performed at 3, 10, and 24 h post-injection of free DOX (a) and Co-NPs (b).

90Plus particle size analyzer and listed in Table 2. Because most amino groups on the mPEG-*b*-PLG-*b*-PLL/DOCA copolymer had been decorated with deoxycholate, the surface charges of the blank and drug-loaded nanoparticles were negative (~ -20 mV). The slightly negative surface charge will contribute to a better blood compatibility and prolonged circulation time of the nanoparticles for the reduced clearance by the reticuloendothelial system (RES) [30].

3.3. Release behavior of drug-loaded nanoparticles

The DOX and PTX release behaviors of Co-NPs were assessed using a dialysis method at 37 °C in phosphate buffered saline (PBS) containing 0.1% Tween 80 at different pH values (7.4 and 5.0). As shown in Fig. 4A, the release of DOX from Co-NPs was greatly affected by the environmental acidity. After a 108 h incubation period, about 24% and 79% of DOX were released at pH 7.4 and 5.0, respectively. The rapid DOX release at pH 5.0 might be attributed to the significantly increased protonation degree of the carboxyl groups in mPEG-*b*-PLG-*b*-PLL/DOCA polymer backbone at a lower pH value, resulting in the weakening of electrostatic interactions between the mPEG-*b*-PLG-*b*-PLL/DOCA nanoparticles and DOX molecules. The release kinetics of PTX from Co-NPs displayed a slow and sustained release pattern at different pH values, and there were no obvious differences between the release rates at pH 7.4 and 5.0 (Fig. 4B). Approximately 67% and 58% of total PTX were released at pH 7.4 and 5.0, respectively. The slow and sustained PTX release from Co-NPs might be ascribed to the strong hydrophobic interaction between PTX and the inner core of the nanoparticles.

3.4. Cellular uptake behavior of the dual-drug loaded nanoparticles

The cellular uptake behavior of Co-NPs was investigated in A549 cells by confocal laser scanning microscopy (CLSM). The cellular nuclei were stained with DAPI (blue), and mPEG-*b*-PLG-*b*-PLL/DOCA copolymers were labeled by FITC (green) for subcellular observation. As shown in Fig. 5B, the green fluorescence was observed in the cells after 1 h incubation. When the incubation period increased to 3 h, the cell uptake of Co-NPs was enhanced and the green fluorescence was distributed widely in the cytoplasm, suggesting that Co-NPs could be successfully internalized by tumor cells *via* endocytosis.

The intracellular DOX release behavior of Co-NPs was also assessed in A549 cells using CLSM. The red fluorescence was performed to visualize the intracellular released DOX (Fig. 5). For both free DOX and Co-NPs, the intracellular DOX fluorescence of 3 h incubation time was stronger than that of 1 h incubation time. For free DOX treated cells, the red fluorescence was observed mostly in the nuclei. Moreover, the DOX fluorescence was distributed both in cytoplasm and nucleus for Co-NPs treated cells at both 1 and 3 h, indicating that Co-NPs were initially located in the intracellular compartments and subsequently released DOX to the nuclei, which was consistent with the subcellular location of Co-NPs. Additionally, cells treated with both free DOX and Co-NPs showed similar DOX accumulation at 1 and 3 h. Considering that free DOX could be quickly transported into cells through the cell membrane *via* a passive diffusion mechanism [31], the results revealed that Co-NPs exhibited a high level of cell uptake through endocytosis.

3.5. *In vitro* cytotoxicity studies

The biocompatibility of the mPEG-*b*-PLG-*b*-PLL/DOCA copolymer was evaluated using MTT assay. A549 (human lung

adenocarcinoma), HeLa (human cervical cancer) and MCF-7 (human breast carcinoma) cell lines were utilized. As shown in Fig. 6, the cell viabilities of A549, HeLa and MCF-7 cells treated with the mPEG-*b*-PLG-*b*-PLL/DOCA nanoparticles at all the tested concentrations up to 1000 $\mu\text{g mL}^{-1}$ after 48 h incubation were all above 85%, indicating that the mPEG-*b*-PLG-*b*-PLL/DOCA copolymer had excellent safety and biocompatibility.

To verify the synergistic effect of the co-delivery system, the *in vitro* antitumor effects of free drugs and drug-loaded nanoparticles against A549 cells were tested using MTT assay. The cell viability histograms were shown in Fig. 7. After 48 h incubation, all free drugs and drug-loaded nanoparticles showed dose-dependent cell proliferation inhibition behavior and the combination of DOX and PTX led to enhanced cell proliferation inhibition. And Co-NPs exhibited the best antitumor activity over a wide range of drug concentrations among all the drug formulations. The IC_{50} values of free drugs and drug-loaded nanoparticles and combination index (CI_{50}) values were summarized in Table 3. The IC_{50} values of DOX-NPs and PTX-NPs were larger than that of free DOX

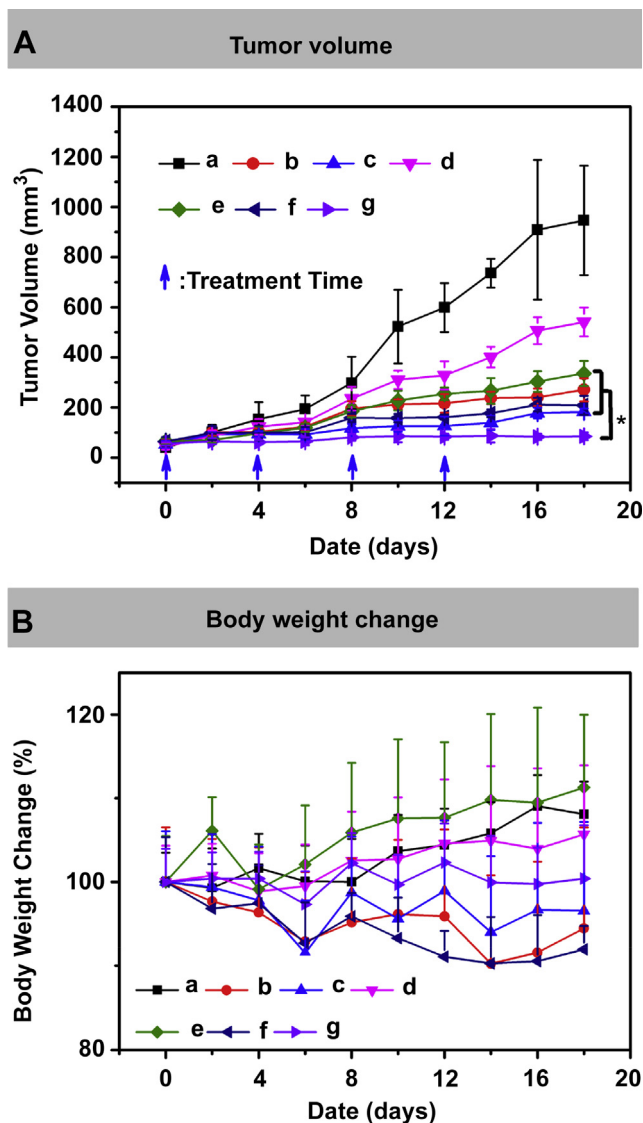


Fig. 9. Tumor volume and body weight changes after anticancer treatment with different drug formulations in nude mice bearing A549 human lung cancer xenograft. Notes: PBS (a), DOX (b), DOX-NPs (c), PTX (d), PTX-NPs (e), DOX + PTX (f) and Co-NPs (g). The data are shown as mean \pm SD ($n = 6$), * $p < 0.01$.

and free PTX, respectively. The reason might be attributed to different cell uptake pathways of free drugs and drug-loaded nanoparticles, and the controlled release manner of drug-loaded nanoparticles. In cell culture medium, most free drugs could quickly display their effects after being transported into cells *via* passive diffusion. However, the drug-loaded nanoparticles were mainly taken up by cells *via* the endocytosis pathway and then

exerted the antitumor activity after the drug molecules were released from the nanoparticles [31]. The CI values lower than, equal to, or higher than 1 indicate synergism, additivity, or antagonism, respectively. The CI_{50} of free PTX + DOX was calculated to be 1.28, which demonstrated that the combination of free DOX and PTX did not receive efficient synergistic effect at the ratio of PTX0.25/DOX. However, the DOX and PTX co-loaded

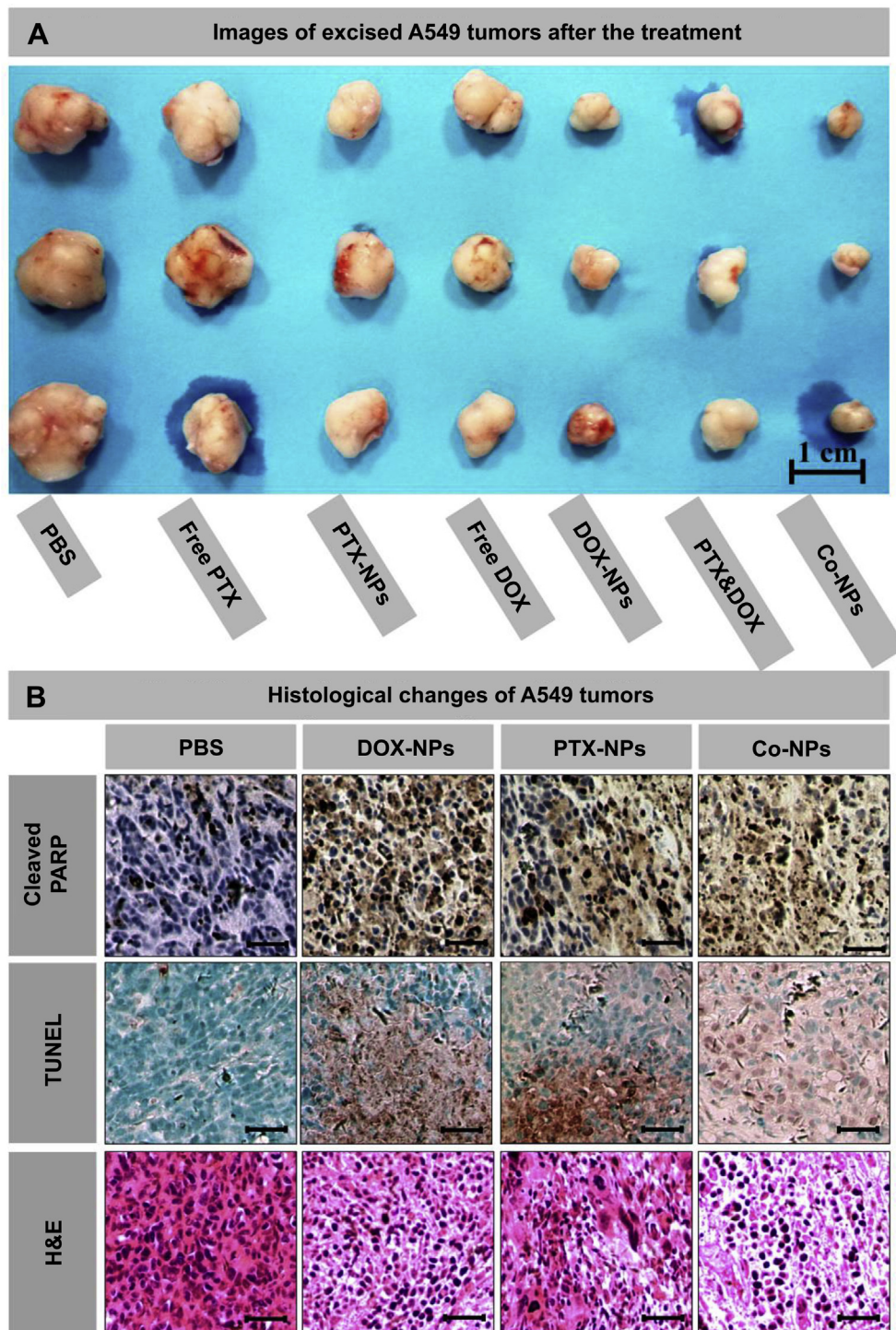


Fig. 10. Images of excised A549 tumors and histological changes of different drug delivery strategies in treatments of A549 human lung cancer implanted in an athymic mouse model. For histological analysis, brown and blue stains represented cleaved PARP1 and nuclei, respectively, in immunohistochemical assay; Green and brown stains indicated normal and apoptotic tumor cells, respectively, in TUNEL analysis; Nuclei were stained violet and extracellular matrix and cytoplasm were stained pink in H&E staining. Scale bars: 100 μ m (For interpretation of the references to color in this figure legend, the reader is referred to the web version of this article.).

nanoparticles showed obvious synergism effect and the CI_{50} value was approximately 0.57, indicating co-delivery of DOX and PTX had evident superiority as compared with free drug combination.

3.6. Excised imaging of free DOX and Co-NPs

To estimate the biodistribution of Co-NPs, *ex vivo* DOX fluorescence imaging of the isolated major organs (heart, liver, spleen, lung, kidney) and tumors at 3 h, 10 h and 24 h post-injection in A549 tumor-bearing nude mice was observed. Free DOX was used as the control group and the representative results were summarized in Fig. 8. As shown in Fig. 8, for free DOX group, DOX fluorescence was mainly observed in kidney at 3 h post-injection and rapidly faded away after injection. The result suggested that the free DOX molecules were metabolized and excreted fast from the body by liver and kidney, which might result in the low drug efficacy and the side toxic effect to the organs. Conversely, the strongest DOX fluorescence was first distributed in liver at 3 h post-injection and then detected mainly in kidney at 10 h post-injection, indicating that Co-NPs exhibited longer blood circulation time. However, stronger fluorescence at tumor site for Co-NPs group was observed in comparison with that for free DOX group at 10 and 24 h. The improved delivery of DOX to tumor for Co-NPs might be attributed to reduced uptake by the RES, the excellent construct stability during the blood circulation and the EPR effect, which would contribute to the enhanced antitumor efficiency.

3.7. *In vivo* antitumor efficiency

On the basis of the above results, the *in vivo* antitumor efficacy and systemic toxicity of the dual-drug loaded nanoparticles were further investigated on A549 human lung tumor-bearing nude mice. Mice were treated with PBS and different drug formulations every four days *via* the intravenous injection, and the tumor volume and the body weight were measured every two days. As shown in Fig. 9A, compared with the rapid tumor growth of PBS treatment group, all the drug formulations showed efficacy in inhibiting the tumor growth to different degrees. For the free drugs and the drug-loaded nanoparticles treated groups, two conclusions could be summarized as follows: (1) The combination of DOX and PTX was more effective than the use of single drug. (2) For the same drugs, the loaded-drug showed better antitumor effect compared with free drug, and the similar results were observed in the drug combination. The best antitumor activity was observed in the Co-NPs treated group, with the almost completely inhibition of tumor growth and no obvious tumor recrudescence during the whole treatment. The tumor volume of Co-NPs treated group was only 9.0% of control group at the end of experiment, which was 3.2-fold, 6.3-fold and 2.4-fold smaller than that treated with free DOX, free PTX and free DOX + PTX, respectively. The superior antitumor effect of Co-NPs might be attributed to the enhanced nanoparticle stability during the blood circulation, the sufficient and instantaneous delivery of two drugs to the tumor site, the efficient cellular uptake in the tumor tissue and the synergistic effect of DOX and PTX on tumor inhibition. The excised A549 tumors after the treatment were dissected and photographed. And the result was consistent (Fig. 10A).

Body weight change is an indicator of systemic toxicity. As shown in Fig. 9B, the body weights of PBS, free PTX and PTX-NPs treated mice showed a continuous and slow increase, which might be partly ascribed to the tumor growth and low toxicity of PTX at the dose of 1 mg kg^{-1} . Obvious weight loss (about 10%) was observed in mice treated with free DOX alone at 4 mg kg^{-1} or in combination with PTX. On the contrary, the treatment with DOX-

NPs or Co-NPs did not lead to any significant body weight loss, demonstrating the reduced systemic toxicity of the loaded drugs. With the high antitumor efficacy and the low drug-related toxicity, the dual-drug loaded system is promising in cancer therapy. The principle of drug combination is to achieve efficient antitumor effect at lower drug doses. Therefore, our next goal is to reduce drug doses to obtain the maximal therapeutic effect and further bring down their side effect.

3.8. Histological and immunohistochemical analyses

To further investigate the antitumor activity of Co-NPs, A549 tumor-bearing nude mice were sacrificed after the treatment (day 18) and the tumors were dissected and stained with H&E, TUNEL and PARP for pathology analysis. The data of PBS, DOX-NPs, PTX-NPs and Co-NPs treated groups were shown in Fig. 10B.

For H&E staining, the normal tumor cells had large nuclei with spherical or spindle shape and more chromatin. Whereas the necrotic cells did not have clear cell morphology, and the chromatin became darker and pyknotic or absent outside the cellular. As shown in Fig. 10B, the tumor cells with normal shape and more chromatin were observed in the PBS group, revealing a vigorous tumor growth. However, the various degrees of tissue necrosis were observed in different drug formulation treated groups. The Co-NPs treated group had larger necrosis area as compared with the groups treated with DOX-NPs and PTX-NPs, indicating that most tumor cells were necrotic in the Co-NPs treated group.

The TUNEL assay could detect DNA fragmentation in the nuclei of tumor cells. Little apoptosis was detected in the PBS treated tumor tissues. While in the DOX-NPs, PTX-NPs and Co-NPs treated groups, obvious cell apoptosis areas were observed. The treatment of Co-NPs obviously increased apoptosis level compared with the signal drug-loaded nanoparticles, which was consistent with the H&E analysis.

Poly-ADP-ribose polymerase (PARP) was one of the essential substrates cleaved by both caspase-3 and -7. The presence of cleaved PARP1 could further detect DNA strand breaks in many cell types [32]. To further confirm the tumor apoptosis, the cleaved 25 kDa fragment of PARP1 was analyzed in the tumor sections by immunohistochemistry. The obvious cleavage products were observed in the tumor tissues treated with various drug-loaded nanoparticles. And compared with DOX-NPs and PTX-NPs treated groups, more cancer cells underwent apoptosis in the group treated with Co-NPs (Fig. 10B).

Together, these data clearly confirmed that the highest level of necrosis and tumor apoptosis was observed in the tumor tissue treated with Co-NPs, which was consistent with the *in vivo* antitumor study.

4. Conclusions

In summary, we developed a polypeptide-based copolymer, mPEG-*b*-PLG-*b*-PLL/DOCA, for the co-delivery of DOX and PTX. The robust construct stability, efficiently delivering capacity, good biocompatibility and favorable size distribution of mPEG-*b*-PLG-*b*-PLL/DOCA revealed its great potential for delivering antitumor drugs *via* intravenous injection in the cancer treatment. FITC-labeled Co-NPs could be successfully internalized by A549 cells tumor cells *via* endocytosis. Co-NPs had synergistic effect in suppression of A549 lung tumor cell growth. Co-NPs exhibited high tumor accumulation, superior antitumor efficiency and much lower toxicity *in vivo*. The present studies indicate that the co-delivery system provides a promising platform as a combination therapy in the treatment of lung cancer, and possible other type of cancer as well. Further studies will be required to investigate an ultimate

dose-dependent response, the optimal doses of both anticancer drugs with maximal anticancer efficacy but less side effect, and the application of this strategy to treat different tumors.

Acknowledgment

This research was financially supported by National Natural Science Foundation of China (Project numbers 51173184, 51373168, 51390484, 51233004 and 51321062), Ministry of Science and Technology of the People's Republic of China (International Cooperation and Communication Program 2011DFR51090), and the Program of Scientific Development of Jilin Province (20130206066GX, 20130727050YY).

References

- [1] Duan XP, Xiao JS, Yin Q, Zhang ZW, Yu HJ, Mao SR, et al. Smart pH-sensitive and temporal-controlled polymeric micelles for effective combination therapy of doxorubicin and disulfiram. *ACS Nano* 2013;7:5858–69.
- [2] Wang H, Zhao Y, Wu Y, Hu YL, Nan KH, Nie GJ, et al. Enhanced anti-tumor efficacy by co-delivery of doxorubicin and paclitaxel with amphiphilic methoxy PEG-PLGA copolymer nanoparticles. *Biomaterials* 2011;32:8281–90.
- [3] Moulder SL, Symmans WF, Booser DJ, Madden TL, Lipsanen C, Yuan L, et al. Phase I/II study of G3139 (Bcl-2 antisense oligonucleotide) in combination with doxorubicin and docetaxel in breast cancer. *Clin Cancer Res* 2008;14:7909–16.
- [4] Han M, Lv Q, Tang XJ, Hu YL, Xu DH, Li FZ, et al. Overcoming drug resistance of MCF-7/ADR cells by altering intracellular distribution of doxorubicin via MVP knockdown with a novel siRNA polyamidoamine-hyaluronic acid complex. *J Control Release* 2012;163:136–44.
- [5] von Minckwitz G, Raab G, Caputo A, Schutte M, Hilfrich F, Blohmer JU, et al. Doxorubicin with cyclophosphamide followed by docetaxel every 21 days compared with doxorubicin and docetaxel every 14 days as preoperative treatment in operable breast cancer: the GEPARDUO study of the German Breast Group. *J Clin Oncol* 2005;23:2676–85.
- [6] Hu C-MJ, Aryal S, Zhang L. Nanoparticle-assisted combination therapies for effective cancer treatment. *Ther Deliv* 2010;1:323–34.
- [7] Zhao Y, Alakhova DY, Kabanov AV. Can nanomedicines kill cancer stem cells? *Adv Drug Deliv Rev* 2013;65:1763–83.
- [8] Wagner E. Programmed drug delivery: nanosystems for tumor targeting. *Expert Opin Biol Ther* 2007;7:587–93.
- [9] Kim S, Shi Y, Kim JY, Park K, Cheng J-X. Overcoming the barriers in micellar drug delivery: loading efficiency, in vivo stability, and micelle-cell interaction. *Expert Opin Drug Deliv* 2010;7:49–62.
- [10] Peer D, Karp JM, Hong S, Farokhzad OC, Margalit R, Langer R. Nanocarriers as an emerging platform for cancer therapy. *Nat Nanotechnol* 2007;2:751–60.
- [11] Gradishar WJ, Tjulandin S, Davidson N, Shaw H, Desai N, Bhar P, et al. Phase III trial of nanoparticle albumin-bound paclitaxel compared with polyethylated castor oil-based paclitaxel in women with breast cancer. *J Clin Oncol* 2005;23:7794–803.
- [12] Barenholz Y. Doxil (R) – the first FDA-approved nano-drug: lessons learned. *J Control Release* 2012;160:117–34.
- [13] Lim WT, Tan EH, Toh CK, Hee SW, Leong SS, Ang PCS, et al. Phase I pharmacokinetic study of a weekly liposomal paclitaxel formulation (Genexol (R)-PM) in patients with solid tumors. *Ann Oncol* 2010;21:382–8.
- [14] Lehar J, Krueger AS, Avery W, Heilbut AM, Johansen LM, Price ER, et al. Synergistic drug combinations tend to improve therapeutically relevant selectivity. *Nat Biotechnol* 2009;27:864.
- [15] Sun TM, Wang YC, Wang F, Du JZ, Mao CQ, Sun CY, et al. Cancer stem cell therapy using doxorubicin conjugated to gold nanoparticles via hydrazone bonds. *Biomaterials* 2014;35:836–45.
- [16] Xiong MH, Tang LY, Wang J. Synthesis and properties of diblock copolymers of poly (ethylene glycol) and poly (2-methoxyethyl ethylene phosphate) for enhanced paclitaxel solubility. *Acta Polym Sin*; 2011:853–60.
- [17] Paridaens R, Biganzoli L, Bruning P, Klijn JGM, Gamucci T, Houston S, et al. Paclitaxel versus doxorubicin as first-line single-agent chemotherapy for metastatic breast cancer: a European Organization for Research and Treatment of Cancer Randomized Study with cross-over. *J Clin Oncol* 2000;18:724–33.
- [18] Dombernowsky P, Gehl J, Boesgaard M, Jensen BW, Ejlersen B, Jensen TP. Treatment of metastatic breast cancer with paclitaxel and doxorubicin. *Semin Oncol* 1995;22:13–7.
- [19] Bourgeois H, Ferru A, Lortholary A, Delozier T, Boisdron-Celle M, Abadie-Lacourtoisie S, et al. Phase I-II study of pegylated liposomal doxorubicin combined with weekly paclitaxel as first-line treatment in patients with metastatic breast cancer. *Am J Clin Oncol* 2006;29:267–75.
- [20] Li MQ, Song WT, Tang ZH, Lv SX, Lin L, Sun H, et al. Nanoscaled poly(L-glutamic acid)/doxorubicin-amphiphile complex as pH-responsive drug delivery system for effective treatment of nonsmall cell lung cancer. *ACS Appl Mater Interfaces* 2013;5:1781–92.
- [21] Lv S, Li M, Tang Z, Song W, Sun H, Liu H, et al. Doxorubicin-loaded amphiphilic polypeptide-based nanoparticles as an efficient drug delivery system for cancer therapy. *Acta Biomater* 2013;9:9330–42.
- [22] Li M, Lv S, Tang Z, Song W, Yu H, Sun H, et al. Polypeptide/doxorubicin hydrochloride polymersomes prepared through organic solvent-free technique as a smart drug delivery platform. *Macromol Biosci* 2013;13:1150–62.
- [23] Ding J, Zhuang X, Xiao C, Cheng Y, Zhao L, He C, et al. Preparation of photo-cross-linked pH-responsive polypeptide nanogels as potential carriers for controlled drug delivery. *J Mater Chem* 2011;21:11383.
- [24] van Dijk-Wolthuis WNE, van de Water L, van de Wetering P, van Steenberghe MJ, Kettenes-van den Bosch JJ, Schuyl WJW, et al. Synthesis and characterization of poly-L-lysine with controlled low molecular weight. *Macromol Chem Phys* 1997;198:3893–906.
- [25] Kim SK, Kim K, Lee S, Park K, Park JH, Kwon IC, et al. Evaluation of absorption of heparin-DOCA conjugates on the intestinal wall using a surface plasmon resonance. *J Pharm Biomed Anal* 2005;39:861–70.
- [26] Chou TC. Theoretical basis, experimental design, and computerized simulation of synergism and antagonism in drug combination studies. *Pharmacol Rev* 2006;58:621–81.
- [27] Ding JX, Chen JJ, Li D, Xiao CS, Zhang JC, He CL, et al. Biocompatible reduction-responsive polypeptide micelles as nanocarriers for enhanced chemotherapy efficacy in vitro. *J Mater Chem* 2013;1:69–81.
- [28] Chen SD, Hu FZ, Sheng RL, Cao AM. Preparation of new cholesterol-based amphiphilic liquid-crystalline diblock copolymers via raft approach and their thermal properties and self-assembly in mixed solutions. *Acta Polym Sin*; 2013:102–11.
- [29] Zhao CL, Winnik MA, Riess G, Croucher MD. Fluorescence probe techniques used to study micelle formation in water-soluble block copolymers. *Langmuir* 1990;6:514–6.
- [30] Du JZ, Du XJ, Mao CQ, Wang J. Tailor-made dual pH-sensitive polymer-doxorubicin nanoparticles for efficient anticancer drug delivery. *J Am Chem Soc* 2011;133:17560–3.
- [31] Prabakaran M, Graier JJ, Pilla S, Steeber DA, Gong SQ. Amphiphilic multi-arm-block copolymer conjugated with doxorubicin via pH-sensitive hydrazone bond for tumor-targeted drug delivery. *Biomaterials* 2009;30:5757–66.
- [32] Bressenot A, Marchal S, Bezdetnaya L, Garrier J, Guillemain F, Plenat F. Assessment of apoptosis by immunohistochemistry to active caspase-3, active caspase-7, or cleaved PARP in monolayer cells and spheroid and subcutaneous xenografts of human carcinoma. *J Histochem Cytochem* 2009;57:289–300.